DOI: 10.1002/ejic.200900537

Anion, Solvent and Time Dependence of High-Spin–Low-Spin Interactions in a 3D Coordination Polymer

Guy N. L. Jameson,*[a] Franz Werner,[b] Matthias Bartel,[c] Alina Absmeier,[c] Michael Reissner,[d] Jonathan A. Kitchen,[a] Sally Brooker,[a] Andrea Caneschi,[e] Chiara Carbonera,[f] Jean-François Létard,[f] and Wolfgang Linert*[c]

Keywords: Spin crossover / Metal-organic frameworks / Anions / Solvent effects

A thorough investigation into the role of the counterion and occluded solvent on the structure and spin-crossover behaviour of the threefold interpenetrated network $[Fe(4\mathit{ditz})_3]^{2+}$ [4*ditz* = 1,4-bis(tetrazol-1-yl)butane] is presented. As seen by X-ray single crystal diffraction, changing the hexafluorophosphate anion in the previously investigated trigonal phase $[Fe(4\mathit{ditz})_3](PF_6)_2$ to tetrafluoroborate causes the butylene spacers to adopt three different conformations, whereupon the symmetry is reduced to triclinic (space group $P\bar{1}$). X-ray powder diffraction and NMR spectroscopy provide evidence for the incorporation of statistically distributed ethanol molecules in the cavities of the compound, whose amount depends on whether absolute ethanol or a binary system, ethanol/water (95:5, v/v), is used as solvent. The phase precipitated from $EtOH/H_2O$ features a metastable high-spin (HS) state when rapidly cooled, a sharp spin transition to a mixed HS/LS (1:1) state at around 90 K on slow cooling with an approximately 10 K hysteresis and LIESST appears, whereas the sample synthesised from absolute ethanol shows a more gradual spin transition at the same temperature without hysteresis.

Introduction

We have recently published structural and magnetic data obtained from a series of spin crossover (SC) ditetrazole complexes with alkylene bridges between the coordinating tetrazoles [1,*n*-bis(tetrazol-1-yl)alkane]. The bridging carbon chain was altered between n = 5–10 and 12 using BF_4^- and n = 4–10 and 12 with ClO_4^- as anion. Absmeier et al.,[1,2] showed, as expected, a decrease in Fe–Fe interactions as the alkylene spacer is extended. This effect is observed through more gradual spin transitions as n is increased. Surprisingly, however, there is in addition a parity effect, which causes the spin-transition temperature (T_{SC} is the temperature of the spin transition estimated from the maximum in the first derivative of the $\chi_M T$ vs. T plot where χ_M stands for the molar magnetic susceptibility) to alternate depending on whether the spacer has an odd or even number of carbon atoms.

Although 1,4-bis(tetrazol-1-yl)butane (4*ditz*) is a member of this class of ligands, the magnetic and magneto-optical behaviour exhibited by its complexes are significantly different. These variations seem to be directly related to structural differences. X-ray powder diffraction (XRPD) has shown that longer-bridged complexes (n = 5–10 and 12) crystallise in a chain-type arrangement. Interestingly, so does $[Fe(2\mathit{ditz})_2](BF_4)_2$[3] where the bridging ligand contains only two CH_2-groups in the spacer. In contrast, 4*ditz* produces a 3D interpenetrating network[4] when PF_6^- is used as anion. $[Fe(4\mathit{ditz})_2](PF_6)_2$ consists of octahedrally coordinated ferrous atoms spanned by the 4*ditz* ligand to produce infinitely long three dimensional networks. Three such networks interpenetrate each other with non-stoichiometric solvent molecules filling cavities present between the faces of iron octahedra of different networks. This complex structure leads to the relatively close proximity of iron atoms and thus enhanced cooperativity between these iron atoms. The coordination polymer is seen to display a sharp two-step spin transition with a hysteresis at approximately

[a] Department of Chemistry, University of Otago, P. O. Box 56, Dunedin, New Zealand
Fax: +64-3-479-7906
E-mail: gjameson@chemistry.otago.ac.nz
[b] College of Science and Engineering, Aoyama-Gakuin University, 5-10-1 Fuchinobe, Sagamihara, Kanagawa 229-8558, Japan
[c] Institute of Applied Synthetic Chemistry, Vienna University of Technology, Getreidemarkt 9/163-AC, 1060 Vienna, Austria
Fax: +43-1-58801-16299
E-mail: wlinert@mail.zserv.tuwien.ac.at
[d] Institute for Solid State Physics, Vienna University of Technology, Wiedner Hauptstraße 8-10/138, 1040 Vienna, Austria
[e] LAMM, Dipartimento di Chimica & UdR INSTM, Università di Firenze, Via della Lastruccia 3, 50019 Sesto F.no, Italy
[f] Institut de Chimie de la Matière Condensée de Bordeaux, UPR CNRS No 9048, Université Bordeaux 1, Groupe des Sciences Moléculaires, 87 Av. du Doc. A. Schweitzer, 33608 Pessac, France
Supporting information for this article is available on the WWW under http://dx.doi.org/10.1002/ejic.200900537.

170 K depending upon the solvent occluded. This cooperativity is in sharp contrast to the other ditetrazole ligands in this series and it is therefore believed that the 4*ditz* ligand is of the optimal length to build such networks.

Previous investigations into $[Fe(4ditz)_2](PF_6)_2$ have also shown a strong solvent dependence of the magnetic properties with minimal changes[5] to the structural parameters. We have therefore, in addition to a detailed structural and magneto-optical analysis, also studied the role of the solvent in $[Fe(4ditz)_2](BF_4)_2$ with a range of techniques including NMR and XRPD and present a study of $[Fe(4ditz)_2](BF_4)_2$ to try to understand the role of the anion and solvent in both the structural properties and the high-spin–low-spin interactions (cooperativity) of iron(II) complexes formed with the 4*ditz* ligand.

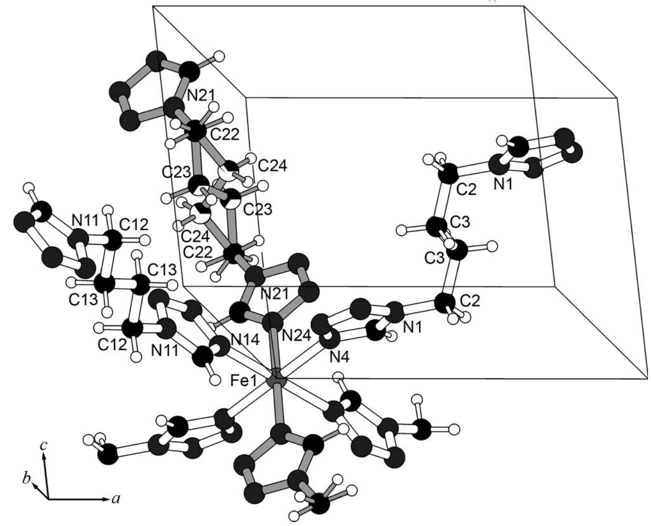

Figure 2. Coordination environment of Fe^{II} in $[Fe(4ditz)_3](BF_4)_2$ synthesised from ethanol/water (95:5%) at 89 K. The disordered 4*ditz*-chain is coloured dark grey; the partially occupied carbon atoms (C23 and C24) are marked with sectors; the unit cell is outlined.

Results and Discussion

Structure

Single-Crystal X-ray Diffraction

$[Fe(4ditz)_3](BF_4)_2$ synthesised by H-tube diffusion from ethanol/H_2O, 95:5% crystallises in the space group $P\bar{1}$ with one formula unit of the complex per unit cell. The crystal structure is similar[4] to $[Fe(4ditz)_3](PF_6)_2$ except for a small distortion in the α-Po-like arrangement of the Fe atoms [see Figure 1 (left) and Figure 3] and the conformation of the butylene spacers (see Figure 2). Three independent networks interpenetrate each other, which have been drawn as cubes for clarity. The anions sit in approximately 1/3 and 2/3 of the face diagonal (slightly left or right) of one cube and are shared with the next one (see Figure 1, right).

Similar to $[Fe(4ditz)_3](PF_6)_2$[4] cavities of approximately 42 $Å^3$ are found between two irons of different networks (along the *c*-axis) which are likely to be filled with non stoichiometric amounts of solvent, though they seem too small to fit ethanol (approx. 50 $Å^3$).[6] The solvent is probably not observed in the crystal data as electron density[5] because, in contrast with $[Fe(4ditz)_3](PF_6)_2$ solvent is present in even smaller amounts (approx. 0.5 mass%, see below) and is statistically distributed. To determine the amount of solvent NMR experiments have been carried out (see below). The

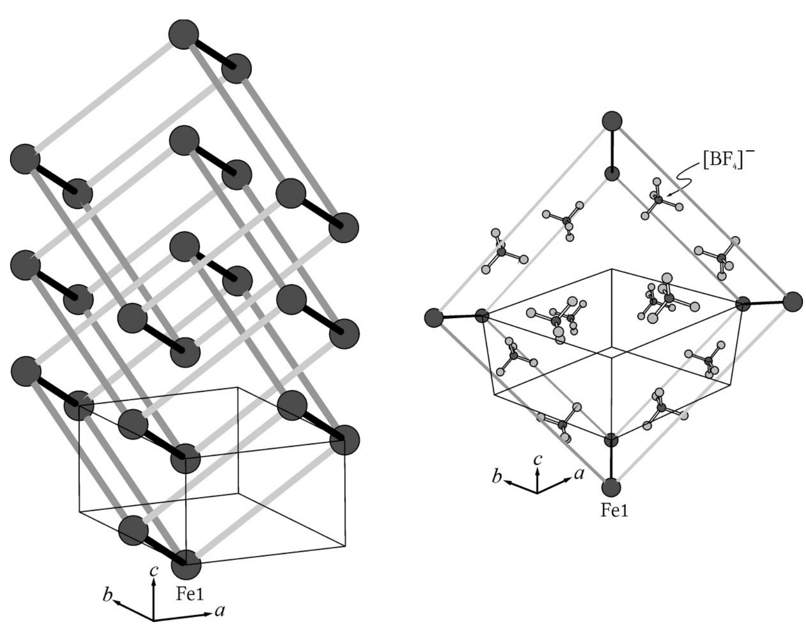

Figure 1. $[Fe(4ditz)_3](BF_4)_2$. Left: scheme of the three interpenetrating networks. The three non-equivalent 4*ditz* ligands are reduced to lines (the disordered ones are coloured dark grey). Right: perspective view along [1 1 –1] of the basal cube with the BF_4^- ions drawn in. The unit cells are outlined.

lower symmetry of $[Fe(4\mathit{ditz})_3](BF_4)_2$ compared with its PF_6-analogue can be seen by the change from 6 equivalent 4*ditz*-chains around the iron in the PF_6-complex into three non-equivalent chains that are doubled by inversion. One chain is staggered in a similar manner to the chains present in $[Fe(4\mathit{ditz})_3](PF_6)$,[4] while one is eclipsed and one is disordered. The disordered chain has two possible alignments with an occupation ratio of 65:35% at 89 K and 50:50% at room temperature which is shown with sectors (for 89 K) in Figure 2. As the spin transition on cooling occurs at a slightly lower temperature (80 K, see SQUID) than that accessible with our single crystal diffraction set-up only a small decrease in the iron–nitrogen bond lengths could be observed [(d_{mean}, 298 K, 89 K) = 2.191 Å, 2.179 Å]. Pertinent information from the crystal data for both temperatures is given in Table 1. Note that a feature of both temperatures is that three fluorine's of the BF_4^- interact in what appears to be a F···π manner with an N of a tetrazole ring (ca. 3 Å); Related interactions have recently been published.[7–10]

Table 1. Selected crystallographic data of $[Fe(4\mathit{ditz})_3](BF_4)_2$ synthesised from ethanol/water (95:5%) at 298 and 89 K.

Empirical formula	$C_{18}H_{30}B_2F_8FeN_{24}$	
Formula weight [g mol^{-1}]	812.13	
Crystal size [mm]	0.15 × 0.10 × 0.07	
Crystal system	triclinic	
Space group	$P\bar{1}$ (No. 2)	
Temperature [K]	298(2)	89(2)
Unit-cell dimensions[a]		
a	8.560(2) Å	8.5016(8) Å
b	10.890(4) Å	10.8815(16) Å
c	10.960(3) Å	10.9066(11) Å
α	60.317(10)°	60.253(5)°
β	84.899(12)°	84.234(6)°
γ	89.648(18)°	89.789(9)°
Volume [Å^3]	883.3(5)	870.34(18)
$\rho_{\text{calcd.}}$ [g cm^{-3}]	1.527	1.549
Radiation/wavelength [Å]	Mo-K_α/0.71073	
μ [mm^{-1}]	0.522	0.530
Max./min. transmission	0.9644/0.9258	0.9639/0.9248
Scan mode	ϕ/ω scans	
$2\theta_{\max}$ [°]	53.84	52.84
Measd./independent rflns.	10002/3698	13271/3523
Rflns. incld. in refinement	3698	3523
σ limits	$I > 2\sigma(I)$	
Absorption correction	semi-empirical from equivalents	
Method of structure Solution/program	Direct methods/SHELXS-97	
Refinement method	Full-matrix least-squares on F^2	
Program	SHELXL-97	
Number of parameters	252	237
Treatment of H atoms		
Final R indices [$I > 2\sigma(I)$]	R_1 = 0.0811 wR_2 = 0.1953	R_1 = 0.0646 wR_2 = 0.1734
R indices (all data)	R_1 = 0.1735 wR_2 = 0.2410	R_1 = 0.0916 wR_2 = 0.1941
Largest diff. peak/hole	1.049/–0.536 e Å^{-3}	1.201/–1.121 e Å^{-3}

[a] For the discussion throughout the paper, the unit cell was transformed and the atomic coordinates were shifted (see below).

If one compares just one cube of the interpenetrating network (at 298 K), where the butylene ditetrazoles are drawn as edges of the cube, it is easily seen that the cube of $[Fe(4\mathit{ditz})_3](PF_6)_2$ is highly symmetrical.[4] The iron–nitrogen distance (Fe–N4) for all six coordinating tetrazoles is the same with a value of 2.193 Å in the HS state. All edges have the same length of 14.381 Å and the angles between the edges have one value of 85.37° (see Table S1 in the Supporting Information). On the other hand $[Fe(4\mathit{ditz})_3](BF_4)_2$ forms a distorted cube. The reason is that not all of the alkylene bridges between tetrazoles which coordinate the Fe (see Figure 2) are stretched out like $[Fe(4\mathit{ditz})_3](PF_6)_2$. The g-edge in Figure 3 represents the ideal orientation of the ligand. Here the alkyl chain is staggered and identical to the $[Fe(4\mathit{ditz})_3](PF_6)_2$ analogue. The torsion angles of the alkylene bridge are $\psi(N^{11}–C^{12}–C^{13}–C^{13})$ = 178.3° and $\psi(C^{12}–C^{13}–C^{13}–C^{12})$ = –180°. The distance between the 2 Fe atoms which are the corners of the cube is 14.468 Å. The distance between the Fe and the coordinating nitrogen N14 is 2.178 Å. The f-edge stands for the eclipsed butylene chain. The distance between the irons is 13.893 Å and the torsion angles are $\psi(N^1–C^2–C^3–C^3)$ = 71.2° and $\psi(C^2–C^3–C^3–C^2)$ = 180°. The Fe–N4 distance (coordinating nitrogen of the tetrazole ring) is 2.208 Å. The e-edge is 13.293 Å long. In this case the chain is disordered and has torsion

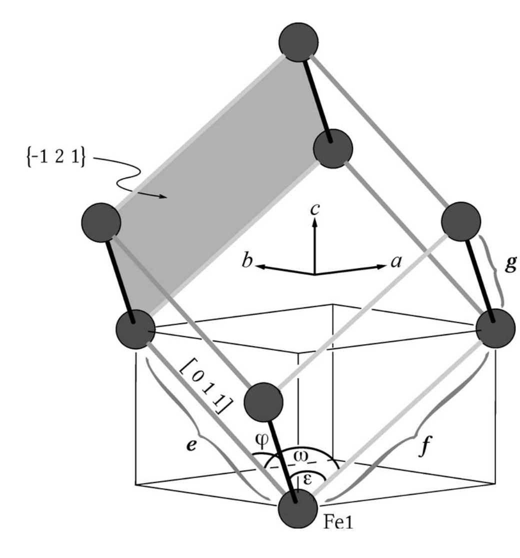

Figure 3. The α-Po–like arrangement of iron in $[Fe(4\mathit{ditz})_3](BF_4)_2$, the unit cell is outlined.

Table 2. Torsion angles and selected distances of $[Fe(4ditz)_3](BF_4)_2$ synthesised from ethanol/water (95:5%) at room temperature and iron–nitrogen distance of the coordinating nitrogen of the tetrazole at room temperature.

Code	Connectivity	Distance [Å]	Torsion angle ψ [°]	Bond	Bond length d [Å]
g	Fe–(N11–C12–C13–C13–C12–N11)–Fe	14.468	178.3, –180	Fe–N14	2.178
f	Fe–(N1–C2–C3–C3–C2–N1)–Fe	13.893	71.2, 180	Fe–N4	2.208
e	Fe–(N21–C22–C23–C23–C22–N21)–Fe	13.293	65, –180	Fe1–N24	2.186

angles of $\psi(N^{21}–C^{22}–C^{23}–C^{23})$ = 65.3° and $\psi(C^{22}–C^{23}–C^{23}–C^{22})$ = –180°. The distance between Fe and N^{24} is 2.186 Å long. The torsion angles and the Fe–N distances (d) for room temperature are given in Table 2.

X-ray Powder Diffraction

The lattice parameters obtained from single-crystal XRD can be compared with those from XRPD. This was successfully achieved by passing the positions of the first 20 reflections to the ITO program.[11] The best solution was found in the triclinic crystal system, a = 8.56, b = 10.91, c = 10.94 Å, α = 60.2, β = 85.0, γ = 90.0°, V = 881 Å^3, M_{20} = 26, which is in full agreement with the values later determined from a single crystal. The volume is in accordance with one formula unit of the complex per unit cell. As can be readily seen the cell shows pseudo-hexagonal symmetry with parameters lying close to the trigonal phase[4] [Fe(4*ditz*)$_3$](PF$_6$)$_2$ [SG $P\bar{3}$, a = 11.258(6), c = 8.948(6) Å, V = 982(1) Å^3, at 300 K]. To allow better comparison the indexing solution was transformed by the matrix [0 1 0] [0 0 –1] [1 0 0] to a non-standard setting and the atomic coordinates were shifted to place the iron atom on the origin in order to ease the comparison with the parent PF_6^- phase. This transformation has also been applied to the single-crystal data, but not to the presented CIF files (see Supporting Information). Comparative inspection of the relative intensities of the powder patterns of the tetrafluoroborate and the hexafluorophosphate clarified that the BF_4^- complex constitutes a distorted variant of the PF_6^- complex. To confirm the indexing result and to obtain more accurate lattice parameters, Le Bail refinement[12] was carried out utilising the program GSAS.[13] The first refinement trials with profile function No. 3 indicated microstrain dominated broadening of the reflections (χ^2 = 26.8). To improve the fit the indices of the anisotropic microstrain axis Y_e [h k l] were permuted in the range –1 to 1 in order to obtain a better match, that was found for the [0 1 1] axis (χ^2 = 20.1). Because the agreement indices were quite poor at this stage it was switched to profile function No. 4 that includes a more sophisticated treatment of anisotropic microstrain broadening.[14] Indeed the refinement converged with R_{wp} = 0.049 and χ^2 = 14.4 (see Figure 4, left). The quite large GoF results from the long counting time/step.[15]

Solvent

X-ray Powder Diffraction

To investigate the influence of solvent and to improve preparation the complex was synthesised using two slightly different solvent systems (ethanol and ethanol/water, 95:5%). When synthesised in absolute ethanol, addition of the iron salt to the ligand solution led to immediate precipitation of the complex. This resulted in different amounts of solvent being trapped within the coordination polymer (see below). The XRPD experiments confirmed that all samples synthesised were single-phase and their intensities were correctly described by the single-crystal structure. Closer inspection of the patterns exhibited significant differences. On changing the solvent from 95:5% ethanol/water mixtures (this proportion was found to yield optimal results in respect to the reflections' breadths) to absolute ethanol the FWHMs increased clearly (Figure 4, right). In addition time-dependent powder patterns of samples obtained in absolute ethanol showed a decrease in the unit-cell volume, caused by a shortened c-axis, which is already visible in the patterns (Figure 5). The lattice parameters are summarised in the Supporting Information, Table S2. This is strongly suggestive that the release of ethanol molecules occurs from cavities arranged along the c-axis, as found in the parent phase [Fe(4*ditz*)$_3$](PF$_6$)$_2$·solv (solv = MeOH or EtOH, see ref.[5] for a detailed discussion).

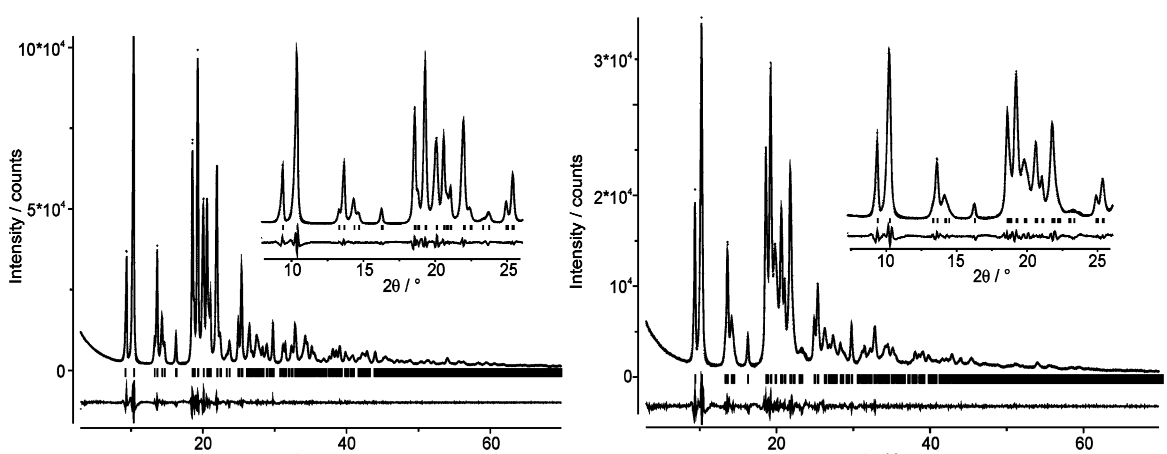

Figure 4. Le Bail refined powder patterns (λ = Cu-$K_{\alpha1,2}$) of [Fe(4*ditz*)$_3$](BF$_4$)$_2$, synthesised from EtOH/H$_2$O, 95:5% (left, χ^2 = 14.4) and abs. EtOH (right, χ^2 = 7.2). The observed and calculated values are drawn with crosses and lines respectively, reflection positions are marked with vertical ticks and the difference curves are shown at the bottom. The regions of the largest d-spacings are inset.

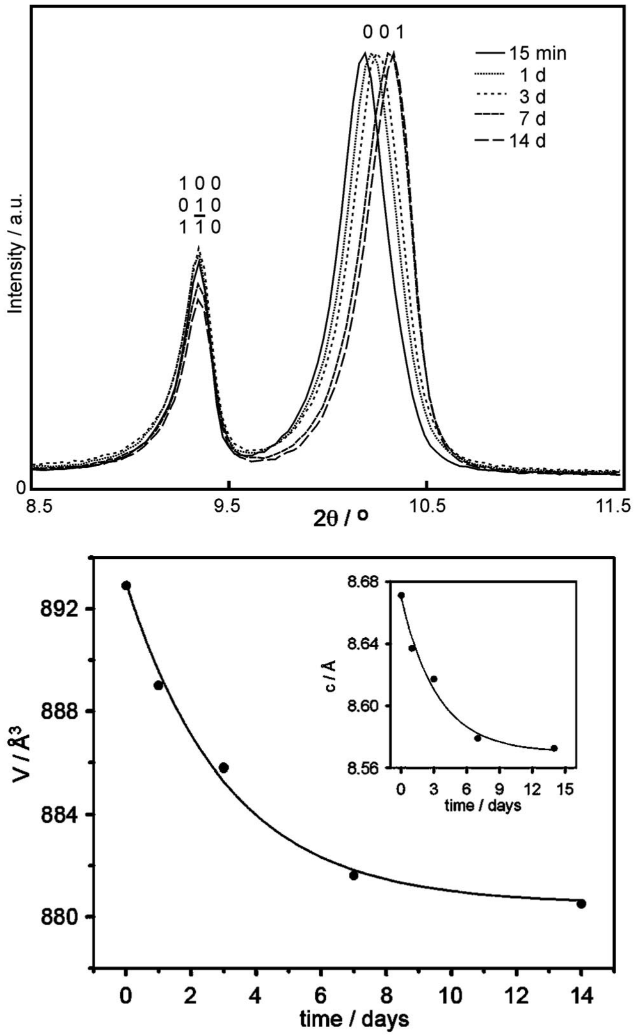

Figure 5. Above: time-dependent shift of the longest diffraction lines (λ = Cu-$K_{\alpha1,2}$) of [Fe(4*ditz*)$_3$](BF$_4$)$_2$, prepared in absolute EtOH. Below: decrease of the unit-cell volume with time. Insert (below) shows the decrease of the *c* axis with time synthesised from absolute EtOH, upon drying.

At this point it is instructive to relate the crystal structure to the lattice-dependent microstrain that can be calculated from the refined profile parameters. In Figure 6 the strain distribution of a 95:5% ethanol/water-precipitated sample is depicted in the three basal zones *h k* 0, *h* 0 *l* and 0 *k l* in percentage terms. Because the curves' principal shape is conserved in the case of the samples precipitated from absolute ethanol, the following introductory considerations also apply. Conspicuous is the considerable difference in microstrain between the *a**- and *b**/*c**-axis, the latter being about 2.9 to 3.5-fold larger. Comparison with the crystal structure (Figure 2) reveals that the *b**/*c**-axes' counterpart in real space frame the e 4*ditz* chain, whose disorder shows up as increased deviations of the corresponding *d*-spacings. This proposal is supported by the observation that the lattice planes of maximum strain are located around {–1 2 1} (Figure 6, D). This plane, spanned by the 4*ditz* chains f and g (Figure 3), is approximately perpendicular to the e chain and turned somewhat sideways from the "ideal" orientation, [0 1 1], of the disordered chain [cf. the order of microstrain (–1 2 1)>(0 1 1)].

The situation is made more complicated when [Fe(4*ditz*)$_3$](BF$_4$)$_2$ is prepared in absolute ethanol, where in addition to the decreasing unit-cell volume a change of microstrain with time is observed. The time-course is shown for the *c*-axis as well as for selected lattice planes (Figure 7, see Supporting Information for all diagrams). Again microstrain is smaller for the {1 0 0} than for the {0 1 0} and {0 0 1} planes. But whereas microstrain decreases with time for {0 0 1}, {0 1 1} and {–1 2 1}, the other planes do not show any noticeable trend. Because it was observed that the disordered e chain is the most flexible one (see above), it is reasonable to conclude that the reduction of microstrain is caused by the loss of ethanol, trapped in the cavities between adjacent iron(II) ions, which is also supported by the decreasing *c*-axis. On losing the solvent the framework adjusts itself by reducing microstrain. It should be noted whilst microstrain-defects are decreased upon the release of ethanol, stacking faults of the iron(II) ions result as seen from increased displacement parameters.

NMR Spectroscopy

The encapsulated solvent molecules have also been detected by NMR spectroscopy using the method described by Bartel et al.[5] Samples were stored in a desiccator under vacuum over P_2O_5 and then dissolved in DMSO and the amount of remaining ethanol detected. This is shown as a ratio of solvent/iron. These measurements were repeated over several days to investigate whether the solvent diffuses out of the polymer and if so how fast.

Samples made from ethanol/water, 95:5% show a very small amount of occluded ethanol (0.04 EtOH/Fe), which remains constant. Single crystals show slightly higher amounts (0.08 EtOH/Fe) and this higher value is consistent with the proposal that the amount encapsulated depends upon the surface/volume ratio.[5]

In contrast, samples synthesised from absolute ethanol show higher initial amounts of occluded solvent which diffuses out over several days (see Figure 8) to finally reach a value of 0.2 EtOH/Fe. This is consistent with the time dependence of the microstrain given in Figure 7.

Of course we cannot exclude that water molecules are also contained within the lattice; detection by NMR-Spectroscopy was not possible and due to the small amounts reliable numbers are difficult to obtain by any method. The presence of water during synthesis is seen to improve crystallinity and could contribute by slowing down precipitation of the product by increasing the solubility of iron. The suggestion that water improves crystallinity through kinetic rather than thermodynamic control is further supported by the fact that only small amounts of solvent are occluded and that absolute ethanol causes immediate precipitation.

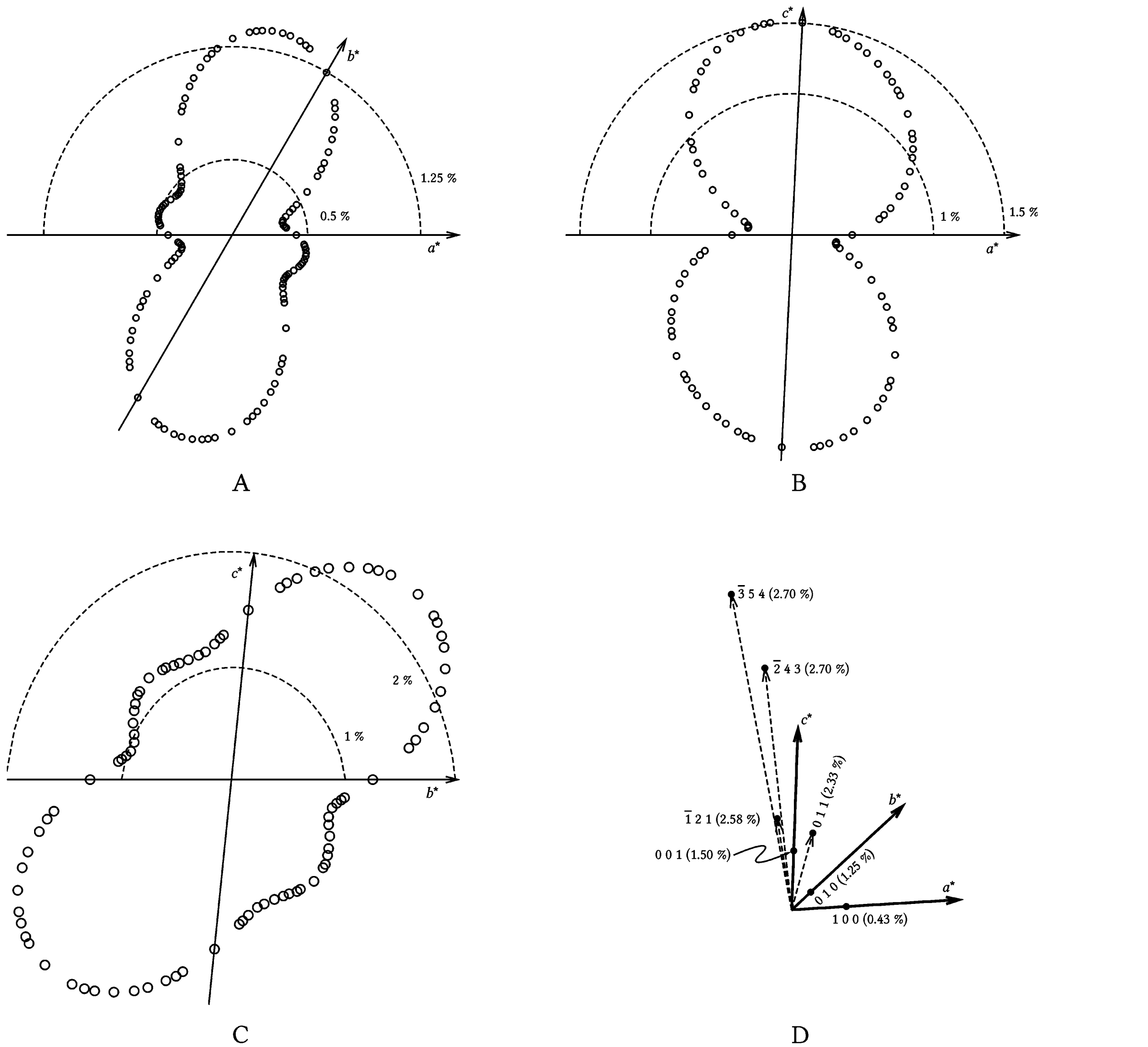

Figure 6. Microstrain distribution of $[Fe(4\mathit{ditz})_3](BF_4)_2$, synthesised from $EtOH/H_2O$, 95:5%, of the zones *h k* 0, *h* 0 *l* and 0 *k l* in reciprocal space (A–C). D shows selected lattice planes with their associated strains.

Magnetic and Photomagnetic Properties

Optical Properties

As expected, the described complex (95:5% $EtOH/H_2O$) shows a thermochromic effect associated with a spin transition, i.e. from white in the HS state at room temperature to violet in the LS state at lower temperatures. This colour change can be detected in the reflectivity experiment, carried out as already described[1,2] and used as a preliminary test for the LIESST experiment. The spectra are measured within the range 450–900 nm at particular temperatures between 10 and 290 K. At room temperature only the HS band at around 830 nm ($^5T_2 \rightarrow ^5E$) is visible whilst at low temperature a band at 570 nm appears, which reflects the LS state ($^1A_1 \rightarrow ^1T_1$). The second LS transition, $^1A_1 \rightarrow ^1T_2$, normally observable at 370 nm, is not within the range of the instrument. Additionally, we recorded the change in intensity of both HS and LS bands as a function of temperature under constant light irradiation (see Supporting Information, Figure S1) by following changes in the reflectivity occurring at 830 ± 2.5 and 550 ± 2.5 nm. In fact, below 80 K, the sample was seen to bleach indicating the occurrence of a LS-HS photoconversion through the LIESST effect. The changes in the HS-band intensity during light irradiation while cycling the temperature are presented in Figure 9. As the system is cooled, the reflectivity at 830 nm reaches a maximum at approximately 70 K and below this temperature bleaching occurs. As the sample is heated again the maximum occurs at approximately 80 K. This seems to indicate the presence of a thermal hysteresis during the spin transition which is confirmed by the SQUID measurements described hereafter. The existence of a hysteresis associated

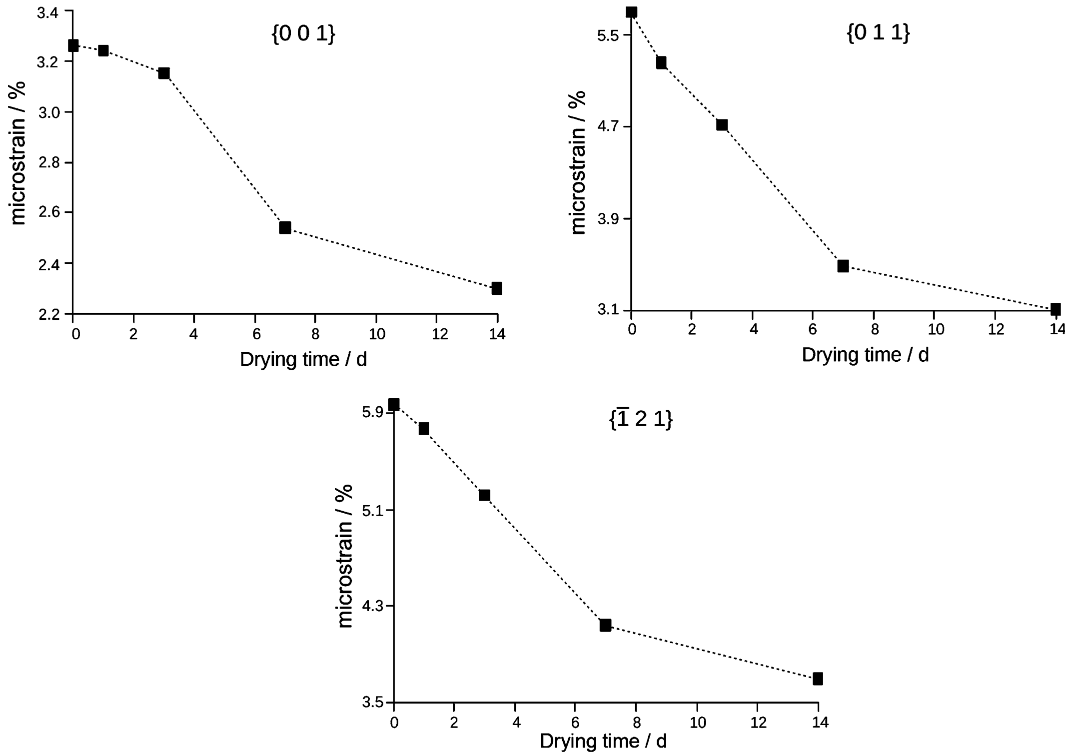

Figure 7. Time-dependent microstrain of [Fe(4*ditz*)$_3$](BF$_4$)$_2$, prepared in absolute ethanol. (The dashed lines serve as a guide to the eyes).

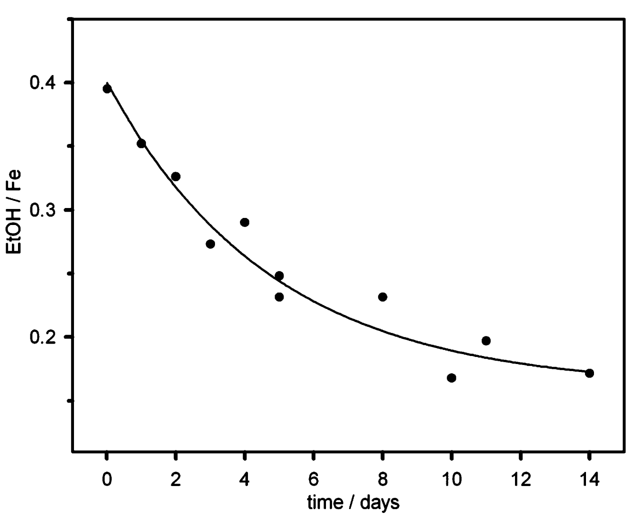

Figure 8. Disappearance of ethanol with time for [Fe(4*ditz*)$_3$]-(BF$_4$)$_2$ from abs. EtOH. The data have been fitted with an exponential function $A_o\exp(-kt)$ + const.

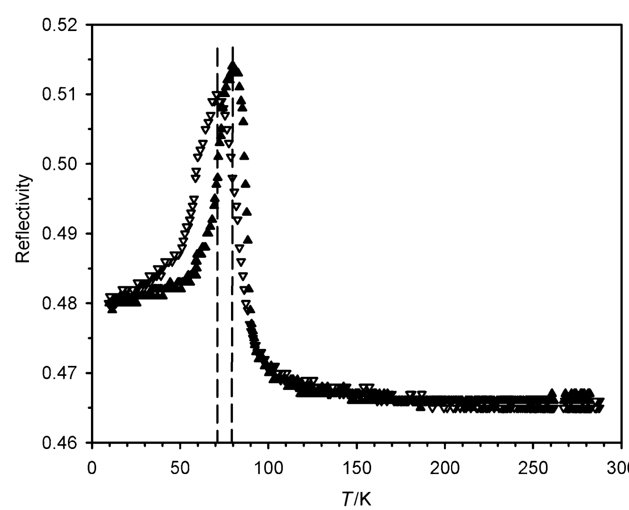

Figure 9. Reflectivity of [Fe(4*ditz*)$_3$](BF$_4$)$_2$ (EtOH/H2O, 95:5%) followed at 830 ± 2.5 nm as a function of temperature. Cooling (∇); warming (▲).

with the LIESST phenomenon corresponds to the LITH (= Light-Induced Thermal Hysteresis) defined by Létard et al.[16] and correlated by Varret et al.[17] to the existence of a cooperative interaction with the lattice. Such a result is confirmed by the existence of a hysteresis loop in the thermal SC regime (see below).

SQUID and LIESST

[Fe(4*ditz*)$_3$](BF$_4$)$_2$ synthesised from EtOH/H_2O, 95:5% (see Figure 10) shows an incomplete spin crossover of approximately 50% of the iron centres with a hysteresis of 9 K (T_{SC} of cooling: 80 K, warming: 89 K). Below 25 K a further sharp decrease of $\chi_M T$ is observed. This drop might be associated with a second spin transition at around 5 K but is unlikely. However this sharp decrease can also be attributed to ZFS. The latter explanation seems to be more likely as the spin state should be frozen at such low temperatures. A similar phenomenon has also been observed by Brooker and co-workers[18–20] using a 1,2,4-triazole-bridged dinuclear Fe^{II} complex with BF_4^- as its anion ($[Fe_2(PMAT)_2](BF_4)_4 \cdot DMF$) and Ksenofontov et al.[21] and Real et al.[22] when discussing the dinuclear $[Fe(bpym)(NCSe)_2]_2$ compound. Irradiation of the sample at 10 K leads to the occurrence of a metastable HS state, which slightly increases with temperature, after the laser is turned off. This increase of $\chi_M T$ can be attributed to ZFS. *T*(LIESST) is determined by the minimum of the first derivative of the $\chi_M T$ vs. T curve during relaxation and gives a value of 63 K. The measurement of the *T*(LIESST) value close to the T_{SC} confirms that the HS residual recorded at low temperature for the $[Fe(4ditz)_3](BF_4)_2$ correspond to a frozen fraction. The *T*(LIESST) limit represents in fact the region where the lifetime of the metastable HS state is very long due to the existence of an activated barrier which slows down the relaxation process. Under such conditions, below *T*(LIESST) the steady value of χ_{HS} could thus be related to the kinetic metastability of the HS state, rather than to a true thermodynamical equilibrium.[23,24]

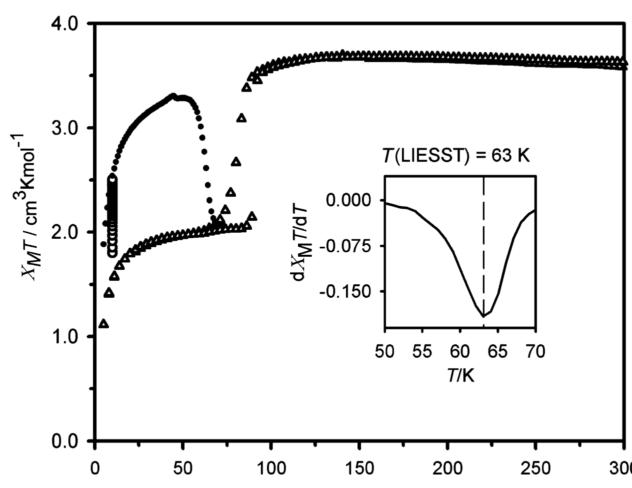

Figure 10. Temperature dependence of $\chi_M T$ for $[Fe(4ditz)_3](BF_4)_2$ ($EtOH/H_2O$, 95:5%) (○) data recorded during irradiation at 10 K; (●) *T* (LIESST) measurement, data recorded in the warming mode with the laser turned off after irradiation for one hour. The existence of a small anomaly at around 50 K on *T*(LIESST) curve corresponds to a remnant oxygen contamination even if particular precaution has been taken to purge the SQUID cavity for one hour at room temperature.

If the sample is cooled rapidly to 10 K from room temperature (taking approx. 5 min) a temperature induced metastable HS fraction can be obtained (see Figure 11). The temperature was then increased at a rate of 0.5 K min^{-1} and the metastable HS state starts to relax to the mixed HS/LS phase at 50 K before returning to the pure HS state at approximately 85 K (see Figure 11 – note that $\chi_M T$ has been converted to mol fraction, see [Equation (1)]).

$$mole\ fraction = \frac{\chi_M T - (\chi_M T)_{\min}}{(\chi_M T)_{\max} - (\chi_M T)_{\min}} \tag{1}$$

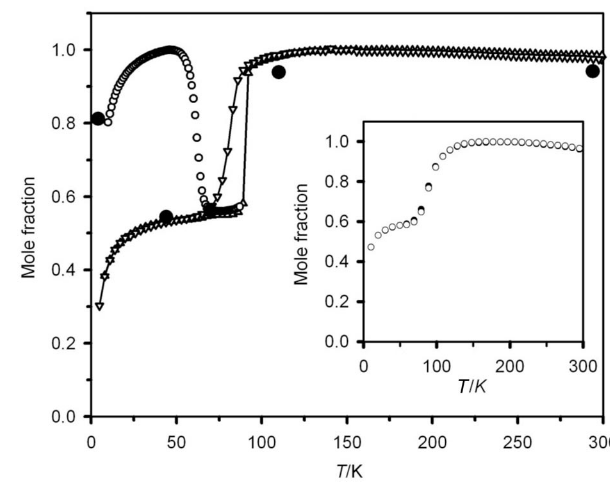

Figure 11. Comparison of the mol fraction of $[Fe(4ditz)_3](BF_4)_2$ ($EtOH/H_2O$, 95:5%) from SQUID (slow cooling ∇; slow warming Δ; warming preceded by rapid cooling ○) and Mössbauer measurement warming preceded by rapid cooling (●). The insert shows the mol fraction [calculated from equation (1)] of $[Fe(4ditz)_3](BF_4)_2$ synthesised from absolute ethanol (slow cooling ●; slow warming ○) between 4 and 300 K.

If the initial cooling rate is decreased (0.5 K min^{-1}) then the transition occurs at 80 K and the mixed HS/LS state is stable down to very low temperatures (see Figure 10 and Figure 11). Slow warming (1.0 K min^{-1}) follows now the same path back except the transition to HS occurs at 89 K equating to a hysteresis of approximately 10 K, which was also observed in the reflectivity experiments (see above).

If the sample is made from absolute ethanol, the magnetic behaviour differs slightly and is shown in the insert in Figure 11 (the data are presented as a mole fraction to aid comparison). The shape of the curve is identical to that of the ethanol/water compound but shows no hysteresis. Again the plateau of approximately 50% HS/LS is reached at low temperatures. Although more gradual the spin transition occurs exactly in the middle of the hysteresis of the complex formed in ethanol/water, 95:5%.

$[Fe(4ditz)_3](PF_6)_2$ was found to show a hysteresis[5] in the thermal spin transition if methanol rather than ethanol was used. A related structure, $[Fe(4ditz)_3](PF_6)_2$ contains larger cavities than $[Fe(4ditz)_3](BF_4)_2$ (compare 90 Å^3 with 42 Å^3). It could therefore be envisioned that again a smaller solvent (water) in the sample synthesised from $EtOH/H_2O$ (95:5%) is responsible for the presence of a hysteresis during spin crossover.

Mössbauer Spectroscopy

It is well known[25–27] that this light-induced metastable HS state at low temperature can, in some cases, be populated through rapid freezing. To further investigate this phenomenon Mössbauer experiments of the sample synthesised from EtOH/H_2O, 95:5% were carried out at temperatures between 4.2 K and 294 K (see Figure 12 and Table 3). The isomer shifts are consistent for HS and LS iron(II) but have a wider quadrupole splitting than those previously measured for [Fe(4*ditz*)$_3$](PF_6)$_2$.[4] To compare Mössbauer with the SQUID data the latter was converted into mol fraction [see Equation (1)] and plotted in Figure 11. The mol fraction values calculated from the Mössbauer data are within experimental error the same as the SQUID data obtained after fast cooling except for one point measured at 44 K, see below.

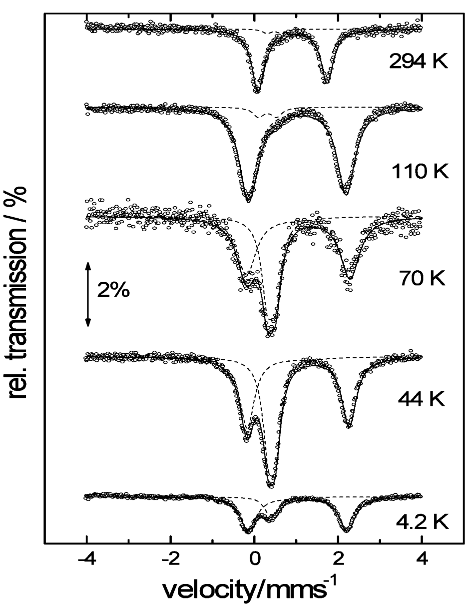

Figure 12. ^{57}Fe-Mössbauer spectra of [Fe(4*ditz*)$_3$](BF_4)$_2$ (EtOH/H_2O, 95:5%) at selected temperatures.

Table 3. Isomer shift (δ) and quadrupole splitting (Δ) obtained for [Fe(4*ditz*)$_3$](BF_4)$_2$ (EtOH/H_2O, 95:5%).

T [K]	A_{LS} (%)	δ(LS) (mm s^{-1}9	Δ(LS) (mm s^{-1})	A_{HS} (%)	δ(HS) (mm s^{-1})	Δ(HS) (mm s^{-1})
4.2	18.8	0.42	0.17	81.2	1.04	2.35
44	45.5	0.42	0.17	54.5	1.05	2.43
70	44.0	0.41	0.19	56.0	1.05	2.47
110	6.2	0.32	0.44	93.9	1.02	2.34
294	5.80	0.30	0.58	94.2	0.92	1.64

In preparation for the Mössbauer experiments the sample is cooled to 4.2 K within 20 min for the first experiment and then the sample is slowly heated for each subsequent experiment. The measurement time at each temperature averages 8 d. The spectrum measured at 4.2 K shows that cooling of the sample is fast enough that most of the sample remains in the HS state (approx. 80%). It also shows that at this temperature the relaxation time of this metastable HS state has a $t_{1/2} > 8$ d and this is confirmed by analysis of intermediate Mössbauer spectra recorded during the 8 d which add together to give the final spectrum given in Figure 12. At 44 K, however, the Mössbauer data show that during the long measurement time the system has relaxed back to the mixed LS/HS state: indeed spectra taken every 12 h show that $t_{1/2} \approx 2$ d.

Complete relaxation during Mössbauer experiments even at 4.2 K has been observed by Yamada et al.[27] when investigating a Fe^{II} complex based on a tripodal ligand with coordinating imidazoles ([$Fe^{II}H_3L^{Me}$]Cl·I_3 where [H_3L^{Me} = tris(2-{[(2-methylimidazoyl-4-yl)methylidene]amino}ethyl) amine]. This complex crystallises in a 2D-layer structure linked by NH–Cl^- hydrogen bonds between the Cl^- ion and three neighbouring imidazole groups. The magnetic measurement shows a metastable HS state caused by rapid cooling but the Mössbauer measurements do not. It seems that the weak inter-layer linking caused by the Cl^- ion means the relaxation time from the metastable HS state is faster than the Mössbauer measurement time. In related compounds Matsumoto, Tuchagues and co-workers[25,26] show 2D networks consisting of two tripodal components tied together by imidazole–imidazolate hydrogen bonds. Here the metastable HS state is observable in both SQUID and Mössbauer measurements. In these cases the relaxation time is longer than the measurement times and this could be because of the stronger hydrogen-bond interactions within the layer. Because the [Fe(4*ditz*)$_3$](BF_4)$_2$ crystallises in a 3D interpenetrating network, rearrangements from HS to LS are large, leading to longer relaxation times at very low temperatures.

Conclusion

Through our systematic study of ditetrazoles it is clear that the particular characteristics of 1,4-bis(tetrazol-1-yl)-butane (in particular its length) are responsible for the formation of a 3D network. If, however, the anion size is decreased (from PF_6^- to BF_4^-), the organic parts of the framework compensate the space deficit by allowing some of the butylene spacers to take other conformations. The basic structure is the same, but the crystal system changes from trigonal ($P\bar{3}$) in [Fe(4*ditz*)$_3$](PF_6) to triclinic ($P\bar{1}$) in [Fe(4*ditz*)$_3$](BF_4). In both cases the anion occupies positions in channels along the *c* axis in between the ligands that lie in the *a*, *b* direction. BF_4^-, being smaller than PF_6^-, forces a shortening of the alkylene chains in two directions. The ligands shorten by adopting an eclipsed and disordered conformation, respectively. The flexibility of the ligand means that the anion thus strongly dictates the structure.

A further important factor is the influence of the solvent upon both the formation of the network and the magnetic properties it exhibits. XRPD data suggest that the solvent is statistically located in 42 Å^3 cavities between two iron atoms of different networks along the *c*-axis. This is suggested by the slow release of solvent (measured by NMR) causing a concomitant small contraction in the *c*-axis as observed by XRPD. The amount of solvent occluded depends on two factors: (i) the volume to surface area ratio – greater amounts are found in single crystals than in the powder form, (ii) the speed of precipitation – in absolute ethanol, the product precipitates quickly out of solution, taking ethanol with it. By addition of 5% water, formation of the network is significantly slower and the structure is more crystalline. Indeed, the increased anisotropic reflection broadening from XRPD exhibited by samples synthesised in absolute ethanol suggests that the speed of formation leads to increased stacking faults, which may explain the increased ethanol observed in these samples.

In particular, $[Fe(4\textit{ditz})_3](BF_4)_2$ shows two interesting effects in its ability (i) to remain in a mixed HS/LS state even at low temperatures and (ii) to remain in a metastable HS state when rapidly cooled, which has a $t_{1/2} \approx 2$ d at 44 K. This first effect has previously been observed in a Fe^{II}–Mn^{II}-cyanide-bridged 1D compound,[28] a Cl^--imidazole-hydrogen-bonded 2D complex[29] and in dimeric SC systems.[18–21,30] The ability to remain in a metastable HS state when rapidly cooled has been noted in a dicyanide iron(II) complex with a macrocyclic Schiff base ligand.[31–34] These results show the important interplay between anion and solvent in the types of structural and magnetic properties observed.

Experimental Section

Chemicals and Standard Physical Characterization: Iron(II) tetrafluoroborate–hexahydrate was obtained from Aldrich. All other chemicals were standard reagent grade and used as supplied. Elemental analyses (C, H and N) were performed in the laboratories of Dr. Roman Boca, Slovenská Vyská Scola Technicá v Bratislave, Chemitechothenologická Fakulta, Radlinského 9, 81237 Bratislava, Slovakia. Mid-range FTIR spectra of the compounds were recorded as KBr pellets within the range of 4400–450 cm^{-1} using a Perkin–Elmer 16PC FTIR spectrometer. Pellets were obtained by pressing the powdered mixture of the samples in KBr in vacuo using a hydraulic press applying a pressure of 10000 $kg\,cm^{-2}$ for 5 min.

Synthesis of the Complex: The general synthetic pathway and the synthesis of the ligand used [1,4-bis(tetrazol-1-yl)butane] (4*ditz*) has been previously reported.[35] The respective ligand [4*ditz*] (1 mmol, 0.194 g) was dissolved in hot ethanol or ethanol/water [95:5% (v/v)]. While the solution cooled to 40 °C iron(II) tetrafluoroborate–hexahydrate (0.33 mmol, 0.111 g) and a small amount of ascorbic acid to preserve the oxidation state of the iron(II) were diluted in ethanol (5 mL). This solution was slowly added to the dissolved ligand and the resulting mixture stirred for four hours. The precipitate was filtered off and the obtained powder was dried with P_2O_5.

Single crystals of the $[Fe(4\textit{ditz})_3](BF_4)_2$ were obtained by H-tube slow diffusion. The ligand (0.65 mmol, 0.126 g) was dissolved in 10–15 mL of hot solvent ethanol/water (95:5%) and placed in one side of the H-tube. On the other side of the tube 10–15 mL of an ethanolic (95:5%) solution containing iron(II) tetrafluoroborate–hexahydrate (0.17 mmol, 0.057 g) was added. The colourless single crystals of the complexes were obtained after fourteen days $\{[Fe(4\textit{ditz})_3](BF_4)_2\}$.

$[Fe(4\textit{ditz})_3](BF_4)_2$: Yield 0.20 g, 73%. $C_{18}H_{30}B_2F_8FeN_{24}$ (812.3): calcd. C 26.62, H 3.72, N 41.40; found C 26.20, H 3.75, N 40.40. Mid-FTIR: $\tilde{\nu}$ = 3148 cm^{-1}. [C–H stretching vibration (ν) of the aromatic tetrazole ring] 2984, 2958 and 2942 cm^{-1} (ν_{C-H} of the aliphatic C–H in the butylene spacer) 1507, 1384 cm^{-1} ($\nu_{N=N}$, ν_{C-N}) 1182, 1101 cm^{-1} ($\nu_{C=N}$, ν_{N-N}, ν_{C-N})

Note: When the sample is synthesised from absolute ethanol instead of ethanol/water (95:5%), it precipitates immediately after the iron salt is added. Because of the loss of the ethanol with time and the analogy of the FIR results (within experimental error) and the detailed PXRD and NMR measurements (see below) where the structure change and the solvent diffusion was analysed, elemental analysis for the compound synthesised from absolute ethanol has not been measured.

X-ray Powder Diffraction (XRPD): The samples were gently ground and placed on a circular single-crystal silicon sample holder of 2.5 cm diameter by the slurry technique using cyclohexane (Merck, p.a.) as elutriating liquid. The diffraction patterns were recorded with a Philips X'Pert diffractometer in Bragg–Brentano geometry, using diffracted-beam-monochromatised Cu-$K_{\alpha1,2}$ radiation, in the angular range 3–70° 2θ with a stepwidth of 0.03° in 2θ. The samples were rotated about the ϕ axis during the measurements.

Single Crystal X-ray Diffraction: The X-ray data were collected at the University of Otago with a Bruker Kappa APEXII area detector diffractometer at 89 and 298 K using graphite-monochromated Mo-K_α radiation (λ = 0.71073 Å). The structures were solved by direct methods using SHELXS-97[36] and refined against F^2 using full-matrix least-squares techniques with SHELXL-97 (Table 1). All non-hydrogen atoms were refined anisotropically. Hydrogen atoms were placed at calculated positions and refined using a riding model with thermal parameters 1.2 times the equivalent isotropic thermal parameters of the attached atom. At both temperatures (89 and 298 K) the iron(II) is located on a centre of inversion and the second half of each of the three half butylene chains in the asymmetric unit is generated by centres of inversion which are located in between the second and third carbon atoms. In one of the three independent chains the second carbon atom is disordered over two sites, [C23:C24 0.65:0.35 at 89 K and C23:C24 0.50:0.50 at 298 K].

CCDC-728144 {for $[Fe(4\textit{ditz})_3](BF_4)_2$ at 89 K}, -728145 {for $[Fe(4\textit{ditz})_3](BF_4)_2$ at 298 K} contain the supplementary crystallographic data for this paper. These data can be obtained free of charge from the Cambridge Crystallographic Data Centre via www.ccdc.cam.ac.uk/data_request/cif.

Reflectivity Measurements: Reflectivity of the samples was investigated by using a custom-built reflectivity set-up equipped with a CVI spectrometer, which allows the collection of both the reflectivity spectra within the range of 450–900 nm at a given temperature and to follow the temperature dependence of the signal at a selected wavelength (±2.5 nm) at 5–290 K. The experiment was performed using directly a thin layer of the powdered sample without any dispersion in a matrix.[37]

Magnetic Susceptibility and Magneto-Optical Measurements: Magnetic measurements were completed on two SQUID magnetometers: (i) SQUID Cryogenix S600 magnetometer with an applied field of 1 T and (ii) a MPMS-55 Quantum Design SQUID magnetometer with an operating field of 2 T. Further measurements were made on a 9 T-PPMS-system from Quantum Design VSM operating with a field of 1 T. All magnetic measurements were performed on powder samples weighting ca. 12 mg. The data were corrected for the magnetisation of the sample holder and for diamagnetic contributions, estimated from Pascal's constants.

The photo-magnetic measurements were performed using a Spectra Physics Series 2025 Kr^+ laser (λ = 532 nm) coupled via an optical fibre to the cavity of the SQUID magnetometer previously described.[38,39] The laser light power at the sample was adjusted to 5 mW cm^{-2}. Bulk attenuation of light intensity was limited as much as possible by the preparation of a thin layer of compound. It is noteworthy that there was no change in the data due to sample heating upon laser irradiation. The weight of these thin layer samples (approximately 0.2 mg) was obtained by comparison of the measured thermal spin-crossover curve with another curve of a more accurately weighed sample of the same compound.

Mössbauer Spectroscopy: The ^{57}Fe Mössbauer spectra were recorded at selected temperatures within 4.2–294 K using a conventional constant acceleration drive system. The source used was ^{57}Co in a Rh-matrix with an activity of about 50 mCi. The data were analyzed using a least-squares fitting procedure assuming Lorentzian lines.[40]

Supporting Information (see also the footnote on the first page of this article): The Supporting Information contains time-dependent edge lengths, angles and lattice parameters, temperature-dependent reflectivity and time-dependent microstrain of selected lattice planes.

Acknowledgments

The authors thank Prof. Kurt Mereiter (Vienna University of Technology, Austria) for XRPD data collection and Prof. Miki Hasegawa (Aoyama-Gakuin University, Japan) for helpful discussions. We also wish to thank Prof. Günter Wiesinger (Vienna University of Technology, Austria) for Mössbauer measurements. M. B. wishes to thank the Marie Curie Training site LAMM (MOLMAG-MEST-CT-2004-504204). Furthermore, we want to thank the European Union (EU COST D14, action project 0011/01) for granting A. A. a "Short Term Scientific Mission" in Bordeaux. We wish to thank the following for financial support: Austrian Science Foundation FWF project (19335-N17), the Italian Ministero dell'Università e della Ricerca (MIUR), Fondo per gli Investimenti della Ricerca di Base (FIRB) (FIRB RBNE033KMA), the European Commission (EC) (NE "MAGMAnet" NMP3-CT-2005-515767 projects) and the MacDiarmid Institute for Advanced Materials and Nanotechnology. Finally, the authors would like to also thank the Aquitaine Region for supporting the development of the ICPA platform (International Center of Photomagnetism in Aquitaine) at the ICMCB.

[1] A. Absmeier, M. Bartel, C. Carbonera, G. N. L. Jameson, P. Weinberger, A. Caneschi, K. Mereiter, J. F. Letard, W. Linert, *Chem. Eur. J.* **2006**, *12*, 2235–2243.
[2] A. Absmeier, M. Bartel, C. Carbonera, G. N. L. Jameson, F. Werner, M. Reissner, A. Caneschi, J. F. Letard, W. Linert, *Eur. J. Inorg. Chem.* **2007**, 3047–3054.
[3] J. Schweifer, P. Weinberger, K. Mereiter, M. Boca, C. Reichl, G. Wiesinger, G. Hilscher, P. J. van Koningsbruggen, H. Kooijinan, M. Grunert, W. Linert, *Inorg. Chim. Acta* **2002**, *339*, 297–306.
[4] C. M. Grunert, J. Schweifer, P. Weinberger, W. Linert, K. Mereiter, G. Hilscher, M. Muller, G. Wiesinger, P. J. van Koningsbruggen, *Inorg. Chem.* **2004**, *43*, 155–165.
[5] M. Bartel, A. Absmeier, G. N. L. Jameson, F. Werner, K. Kato, M. Takata, R. Boca, M. Hasegawa, K. Mereiter, A. Caneschi, W. Linert, *Inorg. Chem.* **2007**, *46*, 4220–4229.
[6] M. Hostettler, K. W. Tornroos, D. Chernyshov, B. Vangdal, H. B. Burgi, *Angew. Chem. Int. Ed.* **2004**, *43*, 4589–4594.
[7] P. D. W. Boyd, C. A. Reed, *Acc. Chem. Res.* **2005**, *38*, 235–242.
[8] M. D. Prasanna, T. N. Guru Row, *Cryst. Eng.* **2000**, *3*, 135–154.
[9] A. Hosseini, M. C. Hodgson, F. S. Tham, C. A. Reed, P. D. W. Boyd, *Cryst. Growth Des.* **2006**, *6*, 397–403.
[10] K. Reichenbacher, H. I. Suss, J. Hulliger, *Chem. Soc. Rev.* **2005**, *34*, 22–30.
[11] J. W. Visser, *J. Appl. Crystallogr.* **1969**, *2*, 89–95.
[12] A. LeBail, H. Duroy, J. L. Fourquet, *Mater. Res. Bull.* **1988**, *23*, 447–452.
[13] A. C. Larson, R. B. Von Dreele, in: *General Structure Analysis System (GSAS)*, Los Alamos National Laboratory Report LAUR, **2004**, pp. 86–748.
[14] P. W. Stephens, *J. Appl. Crystallogr.* **1999**, *32*, 281–289.
[15] R. J. Hill in *The Rietveld Method* (Ed.: R. A. Young), Oxford University Press, Oxford, **1995**, p. 61.
[16] J. F. Letard, P. Guionneau, L. Rabardel, J. A. K. Howard, A. E. Goeta, D. Chasseau, O. Kahn, *Inorg. Chem.* **1998**, *37*, 4432–4441.
[17] A. Desaix, O. Roubeau, J. Jeftic, J. G. Haasnoot, K. Boukheddaden, E. Codjovi, J. Linares, M. Nogues, F. Varret, *Eur. Phys. J., Part B* **1998**, *6*, 183–193.
[18] A. Bhattacharjee, V. Ksenofontov, J. A. Kitchen, N. G. White, S. Brooker, P. Gutlich, *Appl. Phys. Lett.* **2008**, *92*, 174104.
[19] C. M. Grunert, S. Reiman, H. Spiering, J. A. Kitchen, S. Brooker, P. Gutlich, *Angew. Chem. Int. Ed.* **2008**, *47*, 2997–2999.
[20] M. H. Klingele, B. Moubaraki, J. D. Cashion, K. S. Murray, S. Brooker, *Chem. Commun.* **2005**, 987–989.
[21] V. Ksenofontov, H. Spiering, S. Reiman, Y. Garcia, A. B. Gaspar, N. Moliner, J. A. Real, P. Gutlich, *Chem. Phys. Lett.* **2001**, *348*, 381–386.
[22] J. A. Real, I. Castro, A. Bousseksou, M. Verdaguer, R. Burriel, M. Castro, J. Linares, F. Varret, *Inorg. Chem.* **1997**, *36*, 455–464.
[23] C. Balde, C. Desplanches, P. Gutlich, E. Freysz, J. F. Letard, *Inorg. Chim. Acta* **2008**, *361*, 3529–3533.
[24] V. A. Money, C. Carbonera, J. Elhaik, M. A. Halcrow, J. A. K. Howard, J. F. Letard, *Chem. Eur. J.* **2007**, *13*, 5503–5514.
[25] Y. Ikuta, M. Ooidemizu, Y. Yamahata, M. Yamada, S. Osa, N. Matsumoto, S. Iijima, Y. Sunatsuki, M. Kojima, F. Dahan, J. P. Tuchagues, *Inorg. Chem.* **2003**, *42*, 7001–7017.
[26] Y. Sunatsuki, Y. Ikuta, N. Matsumoto, H. Ohta, M. Kojima, S. Iijima, S. Hayami, Y. Maeda, S. Kaizaki, F. Dahan, J. P. Tuchagues, *Angew. Chem. Int. Ed.* **2003**, *42*, 1614–1618.
[27] M. Yamada, E. Fukumoto, M. Ooidemizu, N. Brefuel, N. Matsumoto, S. Iijima, M. Kojima, N. Re, F. Dahan, J. P. Tuchagues, *Inorg. Chem.* **2005**, *44*, 6967–6974.
[28] S. Hayami, G. Juhasz, Y. Maeda, T. Yokoyama, O. Sato, *Inorg. Chem.* **2005**, *44*, 7289–7291.
[29] M. Yamada, H. Hagiwara, H. Torigoe, N. Matsumoto, M. Kojima, F. Dahan, J. P. Tuchagues, N. Re, S. Iijima, *Chem. Eur. J.* **2006**, *12*, 4536–4549.
[30] G. Chastanet, A. B. Gaspar, J. A. Real, J. F. Letard, *Chem. Commun.* **2001**, 819–820.
[31] J. S. Costa, P. Guionneau, J. F. Letard, *Second International Conference on Photo-Induced Phase Transitions: Cooperative, Nonlinear and Functional Properties* **2005**, pp. 67–72.
[32] S. Hayami, Z. Gu, Y. Einaga, Y. Kobayasi, Y. Ishikawa, Y. Yamada, A. Fujishima, O. Sato, *Inorg. Chem.* **2001**, *40*, 3240.
[33] E. Konig, G. Ritter, J. Dengler, S. M. Nelson, *Inorg. Chem.* **1987**, *26*, 3582–3588.
[34] S. M. Nelson, P. D. A. Mcllroy, C. S. Stevenson, E. Konig, G. Ritter, J. Waigel, *J. Chem. Soc., Dalton Trans.* **1986**, 991–995.

[35] P. J. van Koningsbruggen, Y. Garcia, H. Kooijman, A. L. Spek, J. G. Haasnoot, O. Kahn, J. Linares, E. Codjovi, F. Varret, *J. Chem. Soc., Dalton Trans.* **2001**, 466–471.
[36] G. M. Sheldrick, *Acta Crystallogr., Sect. A* **2008**, *64*, 112–122.
[37] C. Carbonera, A. Dei, C. Sangregorio, J. F. Letard, *Chem. Phys. Lett.* **2004**, *396*, 198–201.
[38] J. F. Letard, *J. Mater. Chem.* **2006**, *16*, 2550–2559.
[39] J. F. Letard, P. Guionneau, O. Nguyen, J. S. Costa, S. Marcen, G. Chastanet, M. Marchivie, L. Goux-Capes, *Chem. Eur. J.* **2005**, *11*, 4582–4589.
[40] R. A. Brandt, in: *NORMOS program*, University of Duisburg, Germany, **1999**.

Received: June 16, 2009
Published Online: July 29, 2009